Variations and sources of nitrous acid (HONO) during a severe pollution episode in Beijing in winter 2016

Zhang, Wenqian; Tong, Shengrui; Ge, Maofa; An, Junling; Shi, Zongbo; Hou, Siqi; Xia, Kaihui; Qu, Yu; Zhang, Hongxing; Chu, Biwu; Sun, Yele; He, Hong

DOI:
10.1016/j.scitotenv.2018.08.133

Document Version
Peer reviewed version

Citation for published version (Harvard):
Zhang, W, Tong, S, Ge, M, An, J, Shi, Z, Hou, S, Xia, K, Qu, Y, Zhang, H, Chu, B, Sun, Y & He, H 2019, 'Variations and sources of nitrous acid (HONO) during a severe pollution episode in Beijing in winter 2016', *Science of the Total Environment*, vol. 648, pp. 253-262. https://doi.org/10.1016/j.scitotenv.2018.08.133

Variations and sources of nitrous acid (HONO) during a severe pollution episode in Beijing in winter 2016

Wenqian Zhang[a,b], Shengrui Tong[a,*], Maofa Ge[a,b,c,*], Junling An[d], Zongbo Shi[e], Siqi Hou[a,b], Kaihui Xia[a], Yu Qu[d], Hongxing Zhang[f], Biwu Chu[c,g], Yele Sun[b,c,d], and Hong He[c,g]

[a]*State Key Laboratory for Structural Chemistry of Unstable and Stable Species, CAS Research/Education Center for Excellence in Molecular Sciences, Institute of Chemistry, Chinese Academy of Sciences, Beijing 100190, P. R. China*

[b]*University of Chinese Academy of Sciences, Beijing 100049, P.R. China*

[c]*Center for Excellence in Regional Atmospheric Environment, Institute of Urban Environment, Chinese Academy of Sciences, Xiamen 361021, P. R. China*

[d]*State Key Laboratory of Atmospheric Boundary Layer Physics and Atmospheric Chemistry (LAPC), Institute of Atmospheric Physics (IAP), Chinese Academy of Sciences, Beijing 100029, P. R. China*

[e]*School of Geography Earth and Environmental Sciences, University of Birmingham, Birmingham B15 2TT, United Kingdom*

[f]*Beijing Urban Ecosystem Research Station, State Key Laboratory of Urban and Regional Ecology, Research Center for Eco-Environmental Sciences, Chinese Academy of Sciences, Beijing 100085, P. R. China*

[g]*State Key Joint Laboratory of Environment Simulation and Pollution Control, Research Center for Eco-Environmental Sciences, Chinese Academy of Sciences, Beijing 100085, P. R. China*

Email: tongsr@iccas.ac.cn (S. Tong), gemaofa@iccas.ac.cn (M. Ge)

Abstract

HONO is an important precursor of OH radical and plays a key role in atmospheric chemistry, but its source and formation mechanism remain uncertain, especially during complex atmospheric pollution processes. In this study, HONO mixing ratios were measured by a custom-made instrument during a severe pollution event from 16 to 23 December 2016, at an urban area of Beijing. The measurement was divided into three periods: I (haze), II (severe haze) and III (clean), according to the levels of $PM_{2.5}$. This pollution episode was characterized by high levels of NO (75 ± 39 and 94 ± 40 ppbV during periods I and II, respectively) and HONO (up to 10.7 ppbV). During the nighttime, the average heterogeneous conversion frequency during the two haze periods were estimated to be 0.0058 and 0.0146 h^{-1}, and it was not the important way to form HONO. Vehicle emissions contributed 52% (± 16)% and 40% (± 18)% to ambient HONO at nighttime during periods I and II. The contribution of homogeneous reaction of NO with OH should be reconsidered under high-NO_x conditions and could be noticeable to HONO sources during this pollution event. Furthermore, HONO was positively correlated with $PM_{2.5}$ during periods I and II, suggesting a potential chemical link between HONO and haze particles.

Key words: Nitrous acid measurement, Haze, Vehicle emissions, Homogeneous reaction, Daytime HONO budget

1. Introduction

Hydroxyl (OH) radical is a major oxidant in the troposphere and plays an important role in the ability of the atmosphere to "cleanse itself" (Heard and Pilling, 2003). In addition, OH radical affects many chemical and photochemical processes and contributes to the formation of O_3 and PANs (peroxyacyl nitrates) (Heard and Pilling, 2003; Hofzumahaus et al., 2009). As an important precursor of OH

radical, HONO is a significant species in the tropospheric photochemistry (Alicke et al., 2002; Kleffmann et al., 2005; Lammel and Cape, 1996). Recent studies proposed that HONO photolysis (R1) produced 34% ~ 56% of OH radical in the whole daytime (Alicke et al., 2002; Hendrick et al., 2014; Kleffmann, 2007; Michoud et al., 2012) and produced about 80% of OH radical in the early morning (Acker et al., 2006). Moreover, in pollution episodes, OH radical is almost generated by HONO photolysis (Aumont et al., 2003; Platt and Perner, 1980).

$$HONO + h\nu\ (300\ nm<\lambda<405\ nm) \rightarrow OH + NO \qquad R1$$

In recent years, HONO has been extensively discussed owing to its ability of initiating and accelerating daytime photochemistry. HONO sources were generally grouped into direct emissions, homogeneous reactions, heterogeneous reactions, surface-absorbed nitric acid and/or particulate nitrate photolysis and soil nitrite emissions (Spataro and Ianniello, 2014, and references therein). Although vehicle emissions contribute to ambient HONO, the relative contribution is controversial, as there are different types of vehicles and various vehicle emission standards (Trinh et al., 2017). The reaction of NO with OH (R2) is widely accepted as a key homogeneous pathway to form HONO, especially when NO and OH are high during the daytime in polluted areas (e.g. Li et al., 2012). Due to the low level of OH radical, this homogeneous reaction was reported to be insignificant during the nighttime (Wong et al., 2011). However, recent studies found that nocturnal OH radical were relatively high in China, for example, OH radical was mostly above 3×10^5 cm^{-3} in Wangdu in summer 2014. Therefore, homogeneous formation could play an important role in HONO formation (Tan et al., 2017; Tong et al., 2015). Laboratory studies suggested that heterogeneous conversion of NO_2 into HONO is an important HONO source (Ammann et al., 1998; Broske et al., 2003; Finlayson-Pitts et al., 2003; George et al., 2005; Kleffmann et al., 1999; Stemmler et al., 2007), but

the exact mechanisms are unclear. Although substantial field and laboratory studies were carried out to investigate formation mechanisms of HOHO in the troposphere, HOHO sources and their relative contributions to ambient HONO are still unclear, especially under pollution conditions.

$$OH + NO \xrightarrow{M} HONO \quad \text{R2}$$

Beijing, a rapidly developing megacity in China, has been suffering from haze pollution for several years. For example, only during January 2013, the $PM_{2.5}$ level in the urban area of Beijing exceeded the Second Grade National Standard of China (75 μg m^{-3}) for 22 days, meaning that people were exposed to polluted air for nearly the whole month (He et al., 2014). Although the government rapidly took the strict control measures for anthropogenic emissions, such as vehicle control and production restriction measures, substantial amounts of haze events have occurred since 2013. Haze is usually caused by secondary aerosol particles (Guo et al., 2014; Huang et al., 2014; Liu et al., 2017a). Several studies indicated that high level of HONO produced high level of OH radical, resulting in increased secondary aerosols (An et al., 2013; Huang et al., 2014). Therefore, the source and formation mechanism of HONO are crucial for better understanding the atmospheric chemistry during pollution episodes. Numerous field observations were performed to investigate mixing ratios and potential sources of HONO in Beijing (shown in Table 1), but the studies for the level and formation mechanism of HONO during haze episodes are still limited.

Beijing has suffered from a severe haze pollution from 16 to 21 December, in winter 2016. The government issued the first red alert for heavy air pollution in 2016, and rapidly took the most strict control measures for anthropogenic emissions, such as vehicle control and production restriction measures. Hereby, we performed a field measurement of HONO at an urban area of Beijing during 16 to 23 December 2016, including this severe pollution process. Simultaneous trace gases (SO_2, CO,

67 NO, NO_2 and O_3), $PM_{2.5}$, and meteorological parameters were also obtained in this measurement.
68 The objectives of this study are to explore levels and variations of HONO and to evaluate relative
69 contributions of different HONO sources during this pollution event in Beijing.

70 **Table 1.** HONO measurements in Beijing.

Date	Type	HONO/ppbV	reference
May. Jun-Jul. Sep. Dec. 2000	urban	0.7 - 3.0	(Hu et al., 2002)
Jul.-Aug. 2002/2003	urban	1.72	(Wu et al., 2009)
Aug.-Sep. 2004	urban	0.4 - 6.1	(Qin et al., 2006)
9-10 Feb. 2007	urban	0.15 - 9.71	(Spataro et al., 2013)
Jul. 2008-Apr. 2009	urban	0.19 (spring) 0.18 (summer) 0.46 (autumn) 0.48 (winter)	(Hendrick et al., 2014)
22 Feb.-2 Mar. 2014	urban	0.49 - 3.24 (severe haze) 0.28 - 1.52 (clean)	(Hou et al., 2016)
28 Oct.-2 Nov. 2014	urban suburban	0.54 - 2.77 0.18 - 1.23	(Tong et al., 2015)
12-22 Dec. 2015	urban suburban	1.34 (haze) 0.51 (non-haze) 0.79 (haze) 0.44 (non-haze)	(Tong et al., 2016)
22 Sep. 2015- 25 Jul. 2016	urban	2.27 (autumn) 1.05 (winter) 1.05 (spring) 1.38 (summer)	(Wang et al., 2017)

2. Experimental

2.1. Measurement site

The atmospheric HONO mixing ratios and meteorological parameters were measured on the third floor of No.2 building (~ 10 meters above the ground level) at Institute of Chemistry, Chinese Academy of Sciences (ICCAS, 39°59′22.68″N, 116°19′21.58″E) in Beijing. About 480 meters to the south is the Fourth Ring Road. It is a typical urban site and was described in details in previous works (Hou et al., 2016; Tong et al., 2016; Tong et al., 2015). The observation was performed from 16 to 23 December 2016, including a pollution period and a following clean period. In addition, mixing ratios of trace gases (including SO_2, CO, NO, NO_2 and O_3) and $PM_{2.5}$ were simultaneously acquired from Research Center for Eco-Environmental Sciences, Chinese Academy of Sciences (RCEES, 40°00′28″N, 116°20′15″E), 2.8 kilometers northeast from the ICCAS site, which is also adjacent to the Fourth Ring Road and has similar conditions with few spatial differences of NO_2 and NO_x levels from the ICCAS site. Black carbon was measured at the Tower Branch of the Institute of Atmospheric Physics, Chinese Academy of Sciences (IAP, 39°58'54.9078"N, 116°23'4.7904"E), about 5 kilometers southeast from the ICCAS site. The IAP site is between the North Third and Fourth Ring Roads, which is surrounded by condensed population and heavy traffic, and thus it is a typical urban area of Beijing, similar to two sites above.

2.2. Measurement instruments

The atmospheric HONO mixing ratios were conducted using a custom-made HONO analyzer which was described in details elsewhere (Hou et al., 2016; Tong et al., 2016; Tong et al., 2015). Briefly, the principle of HONO analyzer is similar to long path absorption photometer (LOPAP) (Heland et al., 2001; Kleffmann et al., 2002). HONO is fast collected by a two-channel glass stripping coil with an

absorption solution (0.06 M sulfanilamide in 1 M HCl) to form a stable diazonium salt which then reacts with a dye solution [0.8 mM N-(1-naphthyl) ethylenediamine-dihydrochloride]. Then an azo dye is formed and finally pumped into a 50 cm liquid waveguide capillary cell (LWCC). A subsequent detection is performed by an optical absorption spectrometer (Ocean Optics, SD2000). The final HONO concentration is the difference of signals between the two channels. The liquid flow rate is 0.3 mL min^{-1} with a sampling gas flow rate of 1.0 L min^{-1}. The detection limit of the instrument is 200 pptV with a response time of 15 minutes. A side by side intercomparison between the custom-made HONO analyzer and a commercial LOPAP instrument was carried out in our previous study, which certified the accuracy and reliability of HONO analyzer (Hou et al., 2016).

The meteorological parameters consisting of air temperature (T), relative humidity (RH), wind speed (WS) and wind direction (WD) were measured by a vaisala weather transmitter (WXT520). The mixing ratios of SO_2, CO, NO, NO_2, NO_x and O_3 were determined using SO_2 analyzer (Thermo Scientific, Model 43i), CO analyzer (Thermo Scientific, Model 48i), NO_x analyzer (Thermo Scientific, Model 42i) and O_3 analyzer (Thermo Scientific, Model 49i) with detection limits of 1ppbV, 0.05ppmV, 1ppbV and 1ppbV, respectively. Black Carbon was measured using an AE-33 seven-wavelength Aethalometer.

3. Results and discussion

3.1. Temporal variations of meteorological parameters and gaseous species

Fig. 1 gives an overview of $PM_{2.5}$ and meteorological parameters. The levels of $PM_{2.5}$ were used to classify the measurement into three periods. Period I was a haze period from 16 to 19 December when $PM_{2.5}$ were mostly higher than 75 μg m^{-3} with a mean value of 130 μg m^{-3}, the RH ranged from 22% to 66% and wind speed was from 0 to 1.9 m s^{-1}. Period II was from 20 to 21 December, called a

severe haze period with $PM_{2.5}$ between 140 and 418 μg m^{-3} and the mean value of 285 μg m^{-3}. The RH during period II was between 69% and 88% and wind speed was from 0.1 to 2.2 m s^{-1}. During two haze periods, the wind speed was mostly less than 2.0 m s^{-1}. Due to the strong winds during period III from 22 to 23 December, the air was clean with $PM_{2.5}$ less than 10 μg m^{-3} and the RH less than 30%. Moreover, the RH was negatively correlated with the ambient temperature in general. And most of the observed days had southerly winds, except for 22 December with a strong wind blowing from north-east.

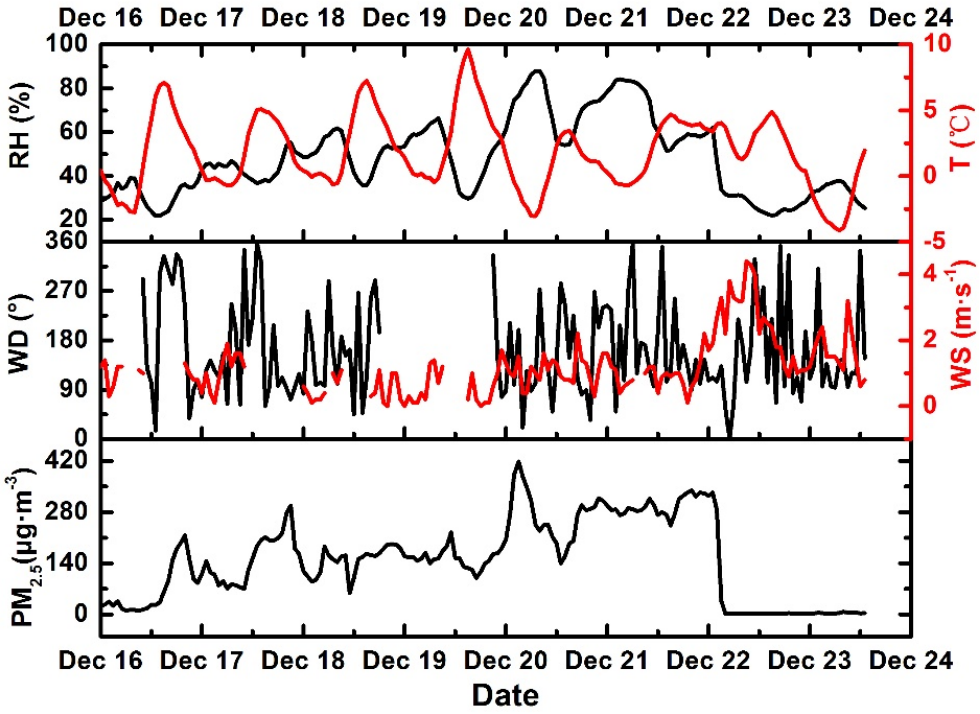

Fig. 1. Temporal trends of hourly average RH, T, WD, WS and $PM_{2.5}$ during the measurement.

The temporal variations of measured trace gases are illustrated in Fig. 2. All the data are hourly averaged. This pollution episode was characterized by high levels of NO_x. The mixing ratios of NO were extremely high with a maximum of 214 ppbV and a mean mixing ratio of 67 ppbV. The NO_2 mixing ratios simultaneously ranged from 8 to 100 ppbV with a mean mixing ratio of 56 ppbV. The SO_2 mixing ratios varied from 1 to 28 ppbV with a mean mixing ratio of 10 ppbV. The mixing ratios

of O_3 and CO varied from 0 to 27 ppbV and 0 to 8.6 ppmV, respectively. HONO varied from 0.3 to 10.7 ppbV with a mean mixing ratio of 3.5 ppbV, higher than those in previous observations (Hou et al., 2016; Spataro et al., 2013; Wang et al., 2017) in Beijing.

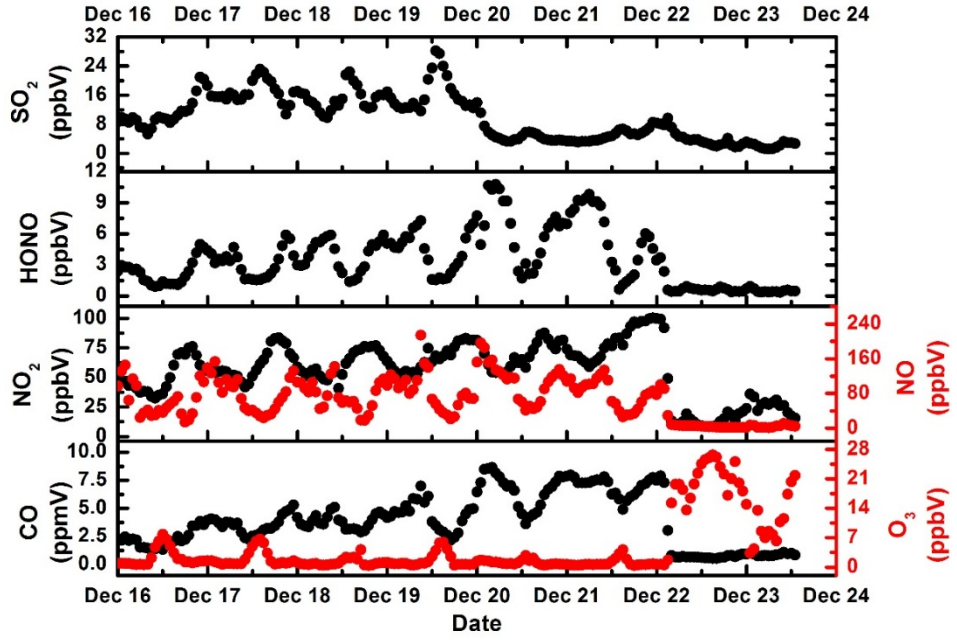

Fig. 2. Temporal variations of hourly average SO_2, HONO, NO_2, NO, CO and O_3 during the measurement.

Table 2 shows mean mixing ratios of trace gases during the three periods. The highest mixing ratios of HONO, NO, NO_2, and CO were found during period II, followed by period I and period III. On the contrary, the O_3 mixing ratios were highest during period III. Furthermore, the SO_2 mixing ratios during period I was much higher than those during period II, with the peak being a factor of ~3 higher, which might be due to the conversion of SO_2 to sulfate (Ma et al., 2018).

Table 2. Mean mixing ratios of trace gases during the three periods.

Trace Gases	I (Haze) 16-19 Dec.	II (Severe haze) 20-21 Dec.	III (Clean) 22-23 Dec.	Total 16-23 Dec.
HONO (ppbV)	3.4 ± 1.7	5.8 ± 3.0	0.5 ± 0.2	3.5 ± 2.7
NO_2 (ppbV)	60 ± 13	76 ± 14	19 ± 9	56 ± 23

NO (ppbV)	75 ± 39	94 ± 40	5 ± 5	67 ± 48
SO_2 (ppbV)	15 ± 4	5 ± 2	3 ± 1	9± 6
O_3 (ppbV)	2 ± 2	1 ± 1	16 ± 7	4 ± 7
CO (ppmV)	3.5 ± 1.2	6.8 ± 1.2	0.8 ± 0.4	3.9 ± 2.3

3.2. Diurnal variations of gaseous species

Fig. 3 illustrates diurnal variations of average HONO, NO_2, NO, SO_2, O_3 and CO during the measurement. The diurnal trends of HONO during the two haze periods I and II were noticeable while those during period III were insignificant, contrary to the measurement in 2014 (Hou et al., 2016) when the variations during clean period were more visible. Such low and stable levels of HONO during period III in this study might be attributed to the strong wind which can accelerate HONO vertical and horizontal mixing. During periods I and II, HONO peaked at around 07:00 LT (local time) (4.6 ppbV) and at around 05:00 LT (10.0 ppbV), respectively. Then HONO mixing ratios gradually decreased, caused by increased HONO photolysis rates and vertical mixing after sunrise (Hendrick et al., 2014). The HONO mixing ratios dropped to minimums (~ 1.4 ppbV) at around 14:00 LT and then accumulated throughout the rest of the day. HONO had a rising process in the evening due to the absence of photolytic loss, the decrease of the boundary layer height and/or strong nocturnal HONO sources (Hendrick et al., 2014). High levels of HONO were found at nighttime. HONO mixing ratio during both periods I and II showed a small decrease before midnight and then increased again from midnight, suggesting potential additional sources. The average diurnal cycles of HONO displayed nocturnal or early-morning maximums and daytime minimums during periods I and II, similar to those in previous studies (Huang et al., 2017; Tong et al., 2016; Wang et al., 2017). The diurnal variations of NO, NO_2, and CO were weak and mixing ratios of these gaseous species were extremely low during period III, due to strong winds. Additionally, diurnal values of NO and

CO followed the same pattern during periods I and II, and peaked at around 9:00 LT due to vehicle emissions during the morning rush hour, subsequently declined to minimums at around 15:00 LT. After 16:00 LT, NO and CO mixing ratios began to rise due to the evening rush hour and the reduction of the boundary layer depth after sunset (Hendrick et al., 2014; Tong et al., 2016). The NO_2 mixing ratios were generally stable and after 12:00 LT gradually increased during periods I and II. But NO_2 mixing ratios exhibited no obvious variations and remained at low levels during period III. SO_2 mixing ratios peaked at around 14:00 LT during two haze periods and their diurnal patterns were more significant during period I than during period II.

According to the descriptions of section 3.1 and 3.2, the wind speed was relatively low during periods I and II, suggesting a limited from regional contribution. However, wind speed was mostly higher than 2.0 m s^{-1} during period III, and severely affected the in situ parameters and thus the data points during period III were not discussed for further analysis of HONO sources in the following sections.

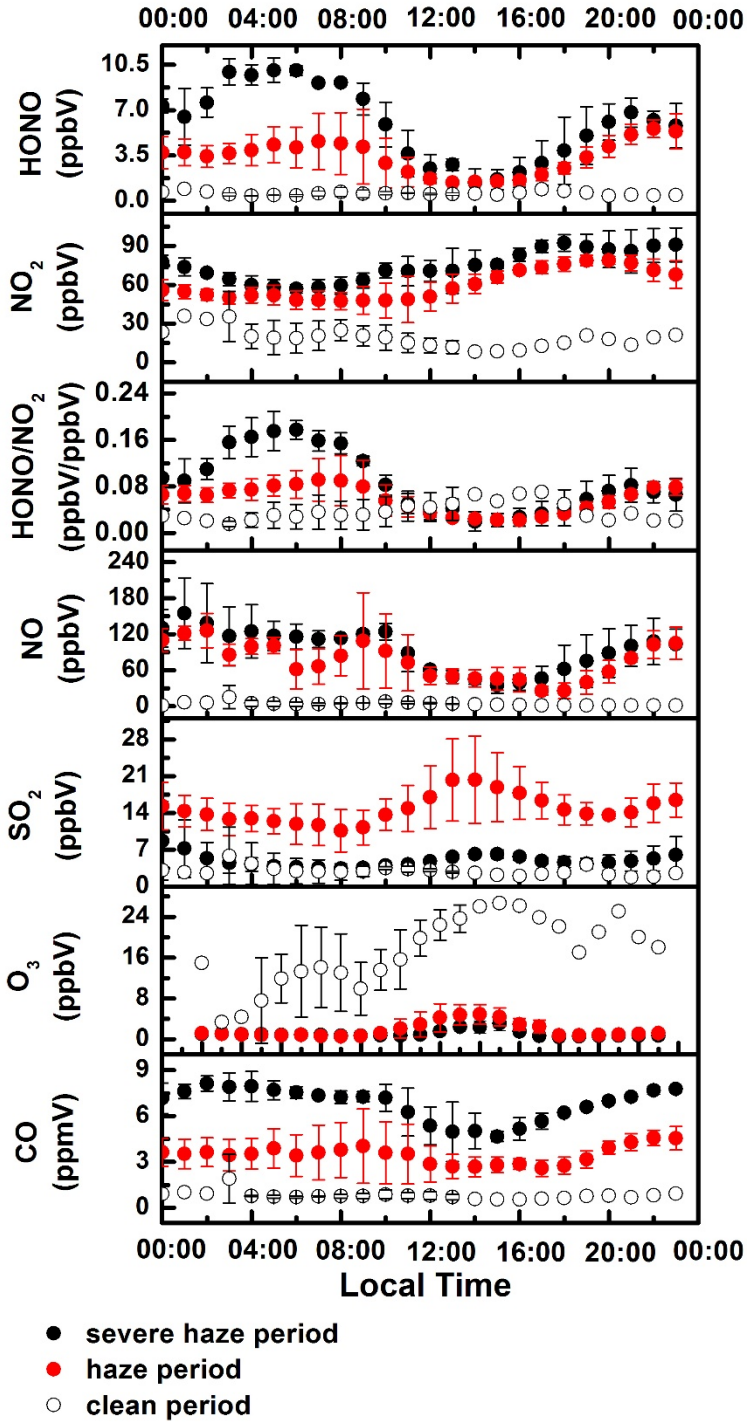

Fig. 3. Diurnal variations of average HONO, NO_2, NO, SO_2, O_3 and CO during periods I (haze), II (severe haze) and III (clean). The error bars represent the standard deviation during the measurement.

3.3. Nocturnal HONO sources

3.3.1 Contribution of homogeneous processes

The net HONO production (P^{net}_{OH+NO}) of homogeneous processes during the nighttime is calculated by

179 the following equation.

180 $P^{net}_{OH+NO} = k_{OH+NO}[OH][NO] - k_{OH+HONO}[OH][HONO]$ (1)

181 $HONO + OH \rightarrow NO_2 + H_2$ R3

182 The rate constants k_{OH+NO} and $k_{OH+HONO}$ are 7.2×10^{-12} and 5.0×10^{-12} cm^3 $molecule^{-1}$ s^{-1}, for reaction
183 R2 and R3 at 298 K, respectively (Li et al., 2012). [NO] and [HONO] are hourly average mixing
184 ratios of NO and HONO, respectively. k_{OH+NO} and $k_{OH+HONO}$ are similar, hence NO and HONO play
185 key roles in calculating P^{net}_{OH+NO}. [OH] is the OH radical concentration which was not available
186 during the measurement, and thus an estimate is made. Tan et al. (2017) observed that the mean value
187 of the nighttime OH was 5×10^5 molecules cm^{-3} in summer 2014 in Wangdu. And here 2.5×10^5
188 molecules cm^{-3} was used, since the $[OH]_{summer}/[OH]_{winter}$ ratio is about 2 (Spataro et al., 2013, and
189 references therein). The nocturnal variations of P^{net}_{OH+NO}, HONO and NO during periods I and II are
190 illustrated in Fig. 4. Generally, the variations of P^{net}_{OH+NO} followed those of NO due to extremely
191 high NO levels governing the variations of P^{net}_{OH+NO} during the two haze periods. During period I,
192 P^{net}_{OH+NO} varied from 0.09 to 0.98 ppbV h^{-1}, and increased before midnight while decreased gradually
193 after midnight. During period II, P^{net}_{OH+NO} ranged from 0.19 to 1.25 ppbV h^{-1} which increased before
194 midnight but decreased after midnight and then almost kept constant. This result implied that the
195 nocturnal HONO source from homogeneous processes was much larger during period II than that
196 during period I. The level of P^{net}_{OH+NO} during the two haze periods were higher than those in previous
197 study by Li et al. (2012) at a rural site in Southern China (0 ~ 0.28 ppbV h^{-1}), but lower than our
198 previous study (2.18 ppbV/h at an urban area of Beijing) (Tong et al., 2015).
199 To estimate the contribution of homogeneous reaction of NO with OH, an episode (17:00 LT ~ 21:00
200 LT) is selected to integrate P^{net}_{OH+NO} with increased HONO mixing ratios. The accumulated HONO

were 3.09 ppbV and 3.90 ppbV from 17:00 LT to 21:00 LT, during periods I and II, respectively. The integrated P^{net}_{OH+NO} and the contributions of homogeneous processes are shown in Table S1. The HONO production from homogeneous reaction contributed 35% and 47% of accumulated HONO, during periods I and II, respectively. And twice and half of 2.5×10^5 molecules cm^{-3} were used for sensitivity studies (Lou et al., 2010) (shown in Table S1). It can be seen that HONO formation at nighttime due to OH and NO homogeneous reaction was highly dependent on the OH concentrations.

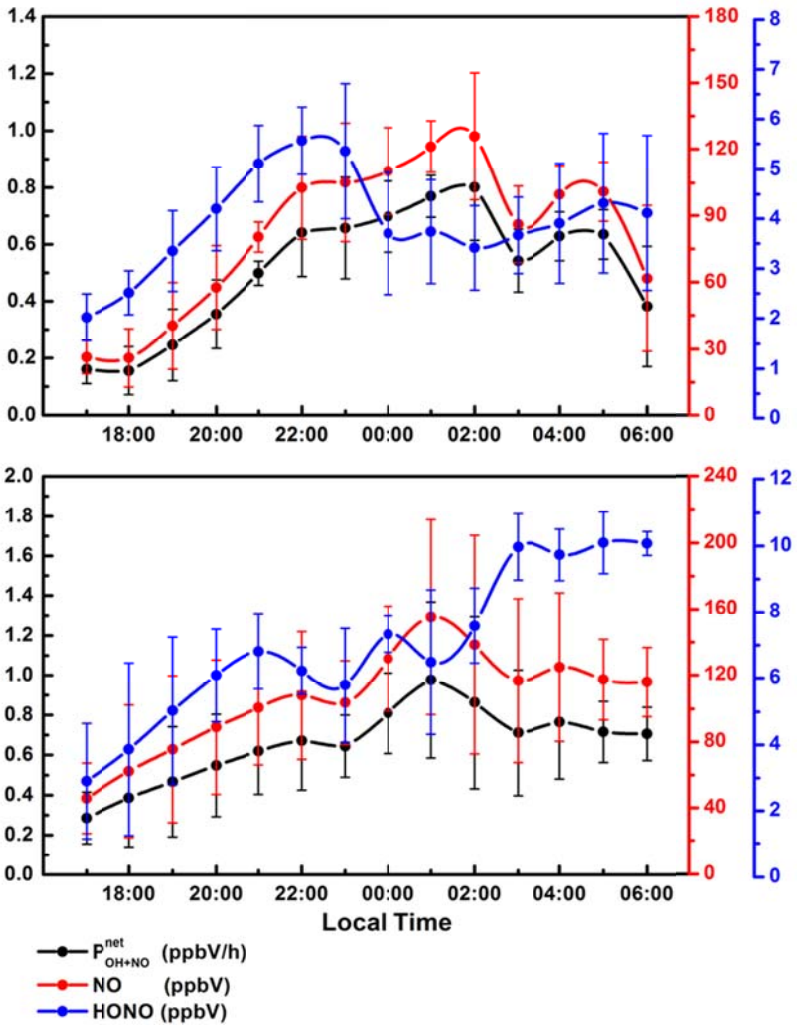

Fig. 4. The nocturnal variations of hourly average P^{net}_{OH+NO}, HONO and NO during periods I and II. The error bars represent the standard deviation.

3.3.2. Heterogeneous conversion of NO_2

Numerous laboratory studies and field observations reported that heterogeneous conversion of NO_2

into HONO frequently occurred in the atmosphere (Spataro and Ianniello, 2014, and references therein). The nocturnal HONO/NO_2 ratios varied from 0.018 to 0.199 during the two haze periods, comparable to the ranges in previous studies (Alicke et al., 2002; Spataro et al., 2013; Tong et al., 2015). The mean values of HONO/NO_2 ratios were 0.064 and 0.095, during periods I and II respectively. HONO conversion frequency is another parameter to evaluate heterogeneous conversion of NO_2 into HONO and is calculated using the following equations and adopting CO and NO_2 as reference gases, as reported by previous studies (Su et al., 2008; Wang et al., 2017).

$$C_{HONO}^{X} = \frac{2\left(\frac{[HONO]_{t2}}{[X]_{t2}} \times \overline{[X]} - \frac{[HONO]_{t1}}{[X]_{t1}} \times \overline{[X]}\right)}{(t_2-t_1)\left(\frac{[NO_2]_{t2}}{[X]_{t2}} \times \overline{[X]} + \frac{[NO_2]_{t1}}{[X]_{t1}} \times \overline{[X]}\right)}$$

$$= \frac{2\left(\frac{[HONO]_{t2}}{[X]_{t2}} - \frac{[HONO]_{t1}}{[X]_{t1}}\right)}{(t_2-t_1)\left(\frac{[NO_2]_{t2}}{[X]_{t2}} + \frac{[NO_2]_{t1}}{[X]_{t1}}\right)} \quad (2)$$

$$C_{HONO} = \frac{1}{3}\left(C_{HONO}^{0} + C_{HONO}^{CO} + C_{HONO}^{NO_2}\right) \quad (3)$$

Where C_{HONO} is HONO conversion frequency from NO_2. $[HONO]_t$, $[NO_2]_t$ and $[X]_t$ represent mixing ratios of HONO, NO_2 and reference gases, respectively, at the measuring time t. $\overline{[X]}$ is the average mixing ratio of reference gas during the time interval of t_1 and t_2, C_{HONO}^{X} is the conversion frequency scaled with X and C_{HONO}^{0} is the conversion frequency which is not scaled. The average C_{HONO} during periods I and II were 0.0058 and 0.0146 h^{-1}, respectively, which were comparable to previous works, such as 0.007 h^{-1} in Shanghai (Wang et al., 2013), 0.008 h^{-1} in Beijing (Wang et al., 2017), 0.014 h^{-1} in Kathmandu (Yu et al., 2009), and 0.0091 h^{-1} in Xi'an (Huang et al., 2017). The higher conversion efficiency of NO_2 heterogeneous reaction was found during period II, which might be attributed to higher RH (69% ~ 88%) (as seen in Fig. S1), since water absorbed on surfaces participated in the heterogeneous reaction of NO_2 to form HONO and several studies confirmed that surface adsorbed water was clearly related to the RH (Stutz et al., 2004, and references therein).

Besides the RH, aerosol surface as a media, is another important factor for heterogeneous conversion of NO_2 (Huang et al., 2017; Li et al., 2012). As aerosol surface density is not available in this study, $PM_{2.5}$ concentrations are used as surrogates to estimate the influence of aerosol surface on the heterogeneous conversion of NO_2 to HONO. The correlation of $HONO/NO_2$ with $PM_{2.5}$ concentrations is shown in Fig. 5. The positive correlation of $HONO/NO_2$ with $PM_{2.5}$ indicated the heterogeneous conversion of NO_2 into HONO on aerosol surfaces. However, the relative amount of HONO formed on aerosol surfaces might be small due to the weak correlation (R^2=0.11).

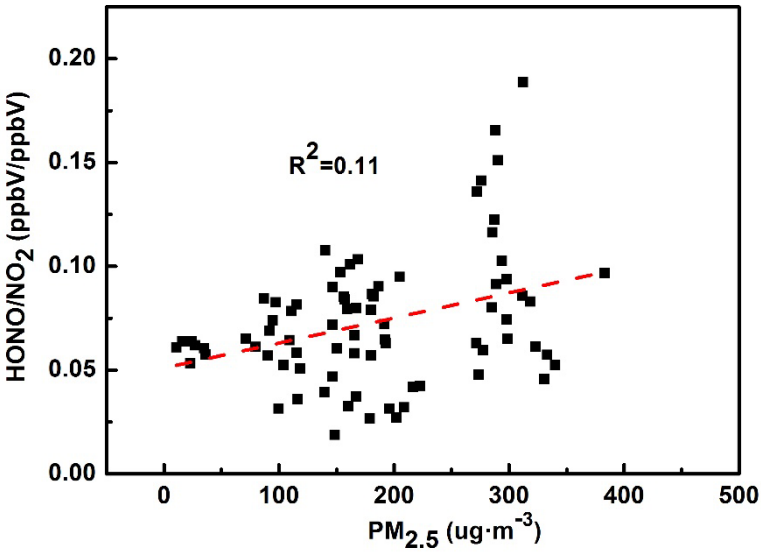

Fig. 5. The correlation of $HONO/NO_2$ ratios with $PM_{2.5}$ during periods I and II.

To further evaluate the contribution of NO_2 conversion, the nocturnal correlations between HONO and NO_2 during periods I and II were illustrated in Fig. 6. There was no significant relationship between HONO and NO_2 during period I while there was a significant negative correlation between them (R^2 = 0.79) during period II. Theoretically, if NO_2 is a critical precursor of HONO, the positive correlation between HONO and NO_2 should be found but that was not the case. This result can be explained by that: some other sources were strong enough and thus they masked the contribution of the NO_2 conversion.

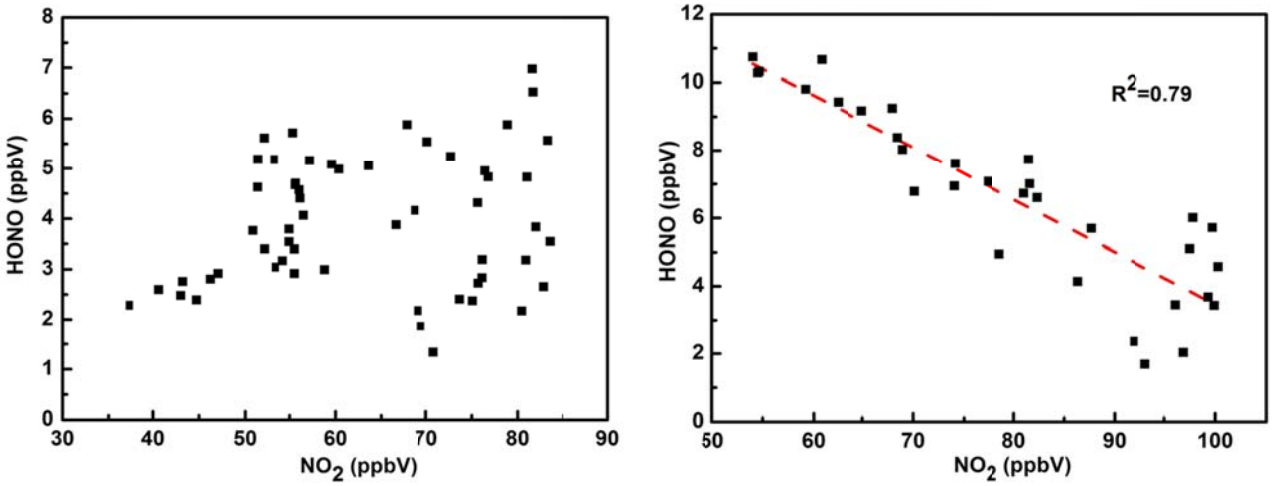

Fig. 6. Correlations of HONO with NO_2 during periods I (left) and II (right).

3.3.3. Contribution of direct emissions

CO and NO are considered as primary pollutants emitted from combustion processes like burning of fossil fuels or biomass as well as vehicle emissions (Quan et al., 2014; Sun et al., 2014; Tong et al., 2016). In this study, good correlations of CO with NO at nighttime during the two haze periods were observed (Fig. S2), indicating that they had common sources. To avoid the influence of HONO photolysis, only the data during the nighttime (from 17:00 LT to next 06:00 LT) was considered. As seen in Fig. 7, the correlations of HONO with CO and NO during the nighttime were 0.70 and 0.27, 0.47 and 0.61 during periods I and II, respectively. It implied that the HONO sources were partly related to those of CO and NO at nighttime. Black carbon (BC) is another primary pollutant typically emitted from combustion processes, such as diesel engines, industry, residential solid fuel, and open burning (Bond et al., 2013). The BC time series during periods I and II is shown in Fig. S3, BC was generally higher during the nighttime than that during the daytime, with peaks at around midnight, resulting from burning coal for heating and diesel vehicles (allowed to enter Fifth Ring Road of Beijing during 23:00 LT~ next 06:00 LT) emissions. The high correlation of HONO with BC (R^2 = 0.49) (Fig. 8) also suggested a possible combustion HONO source, including vehicle emissions.

In urban areas, biomass burning is insignificant and vehicle emissions are important parts of direct emissions (Tong et al., 2016; Nakashima et al., 2017; Ropkins et al., 2017). Hereby, the contribution of vehicle emissions to measured HONO is estimated. The vehicle emissions are calculated by $[HONO_{emission}] = [NO_x] \times K$, where $[HONO_{emission}]$ and $[NO_x]$ are the HONO mixing ratios emitted from vehicle emissions and the observed NO_x mixing ratios, respectively. K is the emission factor. During this haze episode (from 16 to 21 Dec.), the Beijing government issued an odd-even car ban requiring alternate driving days for cars with even- and odd-numbered license plates. It means that vehicle emissions might differ from normal. In order to determine the value of emission factor, we used the nighttime HONO data and simultaneous NO mixing ratios greater than 20 ppbV (Su et al., 2008). With the air aging, the $HONO/NO_x$ ratio gradually increased owing to the conversion of NO_2 to HONO, and thus we use the minimum $HONO/NO_x$ ratio during our measurement period, which is 1.3%, as the emission factor (Li et al., 2012). This is comparable to the result of 1.0% (± 0.5%) reported in Hong Kong by Yun et al. (2017) and in the range of 0.16% ~ 2.1% derived by previous studies (Liu et al., 2017b; Trinh et al., 2017; Kurtenbach et al., 2001). Using this method, the contributions of vehicle emissions to ambient HONO were estimated to be 52% (± 16%) and 40% (± 18%) during periods I and II, respectively. Thus direct emissions from engine exhaust could be an important source of HONO in Beijing.

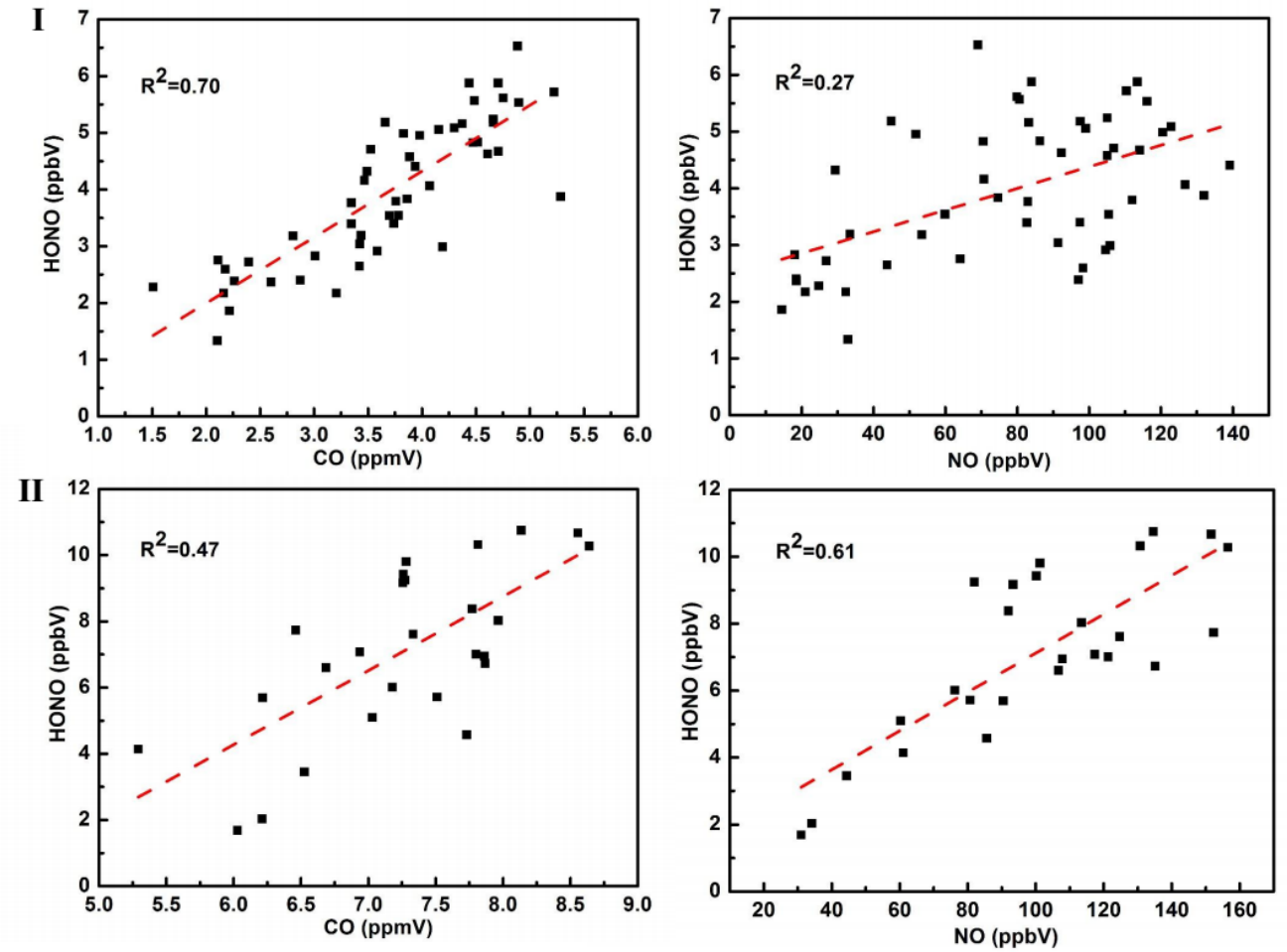

283

284 **Fig. 7.** Correlations of HONO with CO and NO at nighttime during periods I and II.

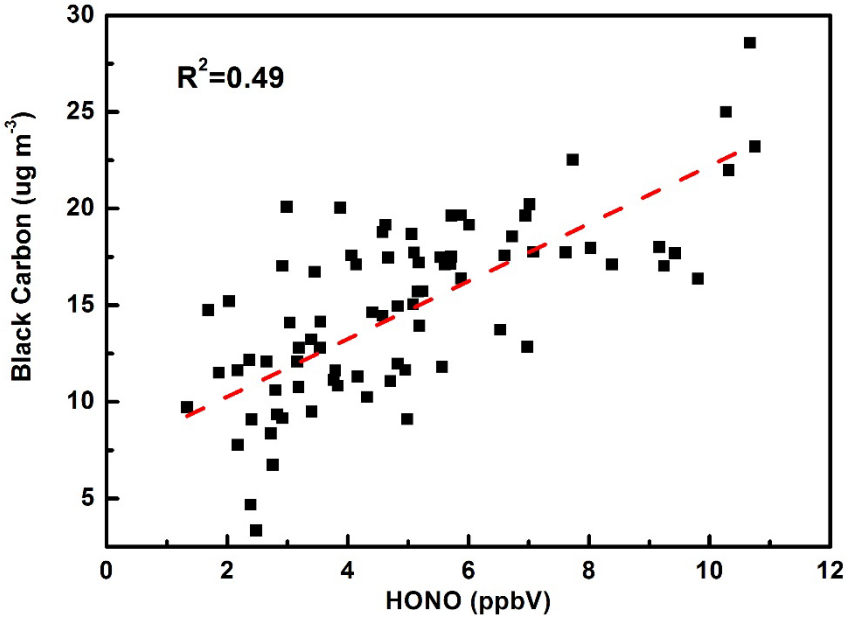

285

286 **Fig. 8.** The correlation of HONO with BC at nighttime during periods I and II.

In summary, the secondary formation of HONO (homogeneous processes and heterogeneous conversion of NO_2) strengthened and primary emissions decreased from period I to period II. Although the heterogeneous conversion of NO_2 contributed to nocturnal HONO, it did not seem to be important. Direct emissions especially vehicle emissions were likely to be a more important source. Moreover, homogeneous processes could also played a noticeable role and should be reconsidered under high-NO_x conditions. In addition, the decrease in the boundary layer height may also contribute to nighttime HONO mixing ratios (Yu et al., 2009), especially before midnight. Thus more relative parameters and further studies are expected to explore the reasons for high levels of HONO at nighttime.

3.4. Daytime HONO budget

During periods I and II, the levels of NO maintained relatively high with a mean mixing ratio of 69 ppbV, indicating that the homogeneous reaction might be significant during the daytime. To support this argument, daytime HONO formation rates during periods I and II can be calculated by the following equation (Soergel et al., 2011):

$$\frac{dHONO}{dt} = \text{sources - losses}$$

$$= (P_{OH+NO} + P_{other}) - (L_{OH+HONO} + L_{photo} + L_{dep}) \quad (4)$$

Such that,

$$P_{OH+NO} + P_{other} = \frac{\Delta HONO}{\Delta t} + L_{OH+HONO} + L_{photo} + L_{dep} \quad (5)$$

Where dHONO/dt represents the variation of measured HONO mixing ratios and can be substituted by $\Delta HONO/\Delta t$. P_{OH+NO} and $L_{OH+HONO}$ represent the homogeneous formation and loss rate of reaction R2 and R3, respectively. The expressions of P_{OH+NO} and $L_{OH+HONO}$ have been discussed in section 3.3.1. P_{other} represents other sources of measured HONO mixing ratios other than the homogeneous

reaction of NO with OH. L_{photo} is the HONO photolysis loss rate of reaction R1, which was calculated by $L_{photo} = J_{HONO} \times [HONO]$, J_{HONO} is the photolysis frequency of HONO. L_{dep} represents the dry deposition of HONO and is expressed by $L_{dep} = V_d \times [HONO] / H$, where V_d is the deposition velocity of HONO and H is the daytime mixing height. V_d was 1.6 cm s^{-1} and H was assumed as 500 m according to previous studies (Hou et al., 2016; Li et al., 2011). Due to the values of OH radicals and J_{HONO} were not available in this study, the NCAR Tropospheric Ultraviolet and Visible (TUV) transfer model (http://cprm.acom.ucar.edu/Models/TUV/Interactive_TUV/) and O_3 column density measured by the Total Ozone Mapping Spectrometer (TOMS, data available at https://ozoneaq.gsfc.nasa.gov/data/ozone/) were used (Huang et al., 2017; Spataro et al., 2013). Considering the effects of aerosol on J values, aerosol optical parameters including aerosol optical depth (AOD), single scattering albedo (SSA) and Angstrom exponent were set as inputs in the TUV model. The typical AOD, SSA and Angstrom exponent values of 1.535, 0.88 and 1.4 were considered, respectively, for the two haze periods I and II (Che et al., 2015; Hou et al., 2016; Jing et al., 2015; Zhang et al., 2014). During the daytime (10:00 LT ~ 15:00 LT), the calculated J_{HONO} values varied from 1.02×10^{-4} to 2.22×10^{-4} s^{-1}, comparable to previous reports (Hou et al., 2016; Huang et al., 2017). Based on the strong correlations of J_{O^1D} (derived by TUV model) with OH radicals, the simultaneous OH concentrations were calculated (Rohrer et al., 2006; Lu et al., 2013). The hourly average OH ranged from 1.66×10^6 to 2.21×10^6 cm^{-3} from 10:00 LT to 15:00 LT during periods I and II, within the range of observed OH in the northern parts of China by Lu et al. and Tan et al. (Lu et al., 2013; Lu et al., 2012; Tan et al., 2017) and comparable to the study (observed OH concentration at noontime of 2.4×10^6 cm^{-3} in severely polluted air from January to March) at a suburban area of Beijing in winter 2016 by Tan et al. (2018).

The average production (P_{OH+NO}) and loss ($L_{OH+HONO}$, L_{dep} and L_{photo}) rates for daytime HONO budget during periods I and II are illustrated in Fig. S4. The mean values of $L_{OH+HONO}$, L_{dep} and L_{photo} were 0.07 ± 0.03, 0.22 ± 0.12 and 1.15 ± 0.61 ppbV h^{-1}, respectively during period I, and 0.11 ± 0.06, 0.34 ± 0.21 and 1.84 ± 1.07 ppbV h^{-1}, respectively during period II. The average P_{OH+NO} were 3.04 ± 1.72 and 3.43 ± 1.66 ppbV h^{-1}, during periods I and II respectively, which is much higher compared to previous reports (Hou et al., 2016; Huang et al., 2017; Wang et al., 2017). Although the P_{OH+NO} has a large uncertainty, it played a key role in daytime HONO budget. And it was even enough to explain the HONO sources during the daytime, if that is the case, there could be one or more important sinks other than HONO photolysis, deposition of HONO and gas-phase reaction of HONO with OH to mediate the discrepancy between sources and sinks of daytime HONO in such complicated pollution periods.

3.5. The correlations between HONO, $PM_{2.5}$ and RH

Fig. 9 illustrates the correlations between HONO, $PM_{2.5}$ and the RH. $PM_{2.5}$ increased with HONO mixing ratios and RH, and had a pronounced correlation with HONO (R^2 = 0.45), suggesting a potential chemical link between HONO and haze particles (An et al., 2013; Huang et al., 2014). Moreover, increased RH is favorable for uptake and mass transport of reactive trace gases, such as SO_2 and N_2O_5, which facilitated reactions of reactive trace gases into particles and accelerating formations of secondary pollutants during heavy haze episodes (Liu et al., 2017a).

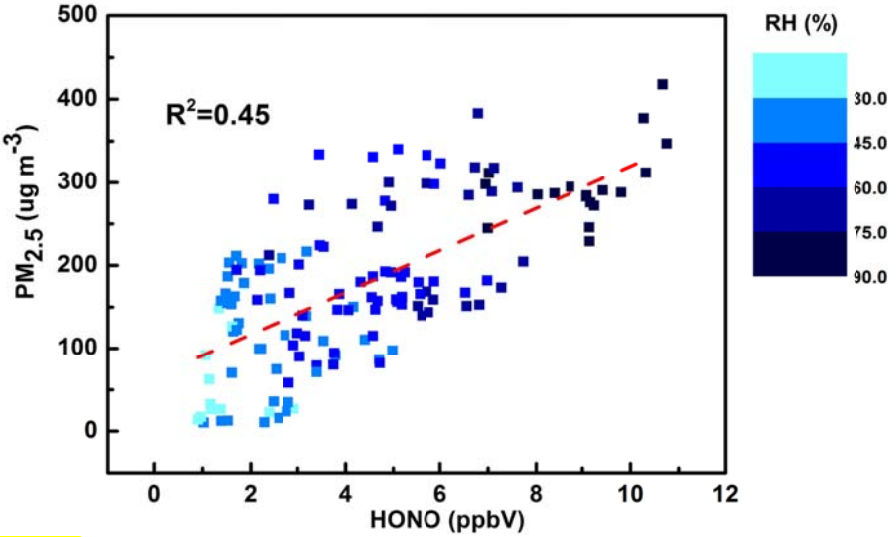

Fig. 9. Correlations between HONO, $PM_{2.5}$ and RH during periods I and II.

4. Conclusions

Atmospheric nitrous acid (HONO) was measured during a severe pollution episode, in Beijing. The mean mixing ratio of HONO during the whole measurement was 3.5 ppbV with a maximum of 10.7 ppbV. The HONO level was much higher than other observations in Beijing during recent years. The measurement was classified into haze (I), severe haze (II) and clean (III) periods. Vehicle emissions contributed 52% (± 16)% and 40% (± 18)% of the nighttime HONO during periods I and II, respectively and could be important HONO sources during this haze episode. Moreover, the heterogeneous conversion of NO_2 did not seem to be important at nighttime. The contribution of homogeneous reaction of NO with OH should be reconsidered and might be crucial under high-NO_x conditions. And poorer dispersion conditions may also contributed to high HONO mixing ratios during this haze event. More studies are required to accurately estimate not only HONO sources but also HONO sinks in the real atmosphere. In addition, an obvious correlation between HONO and $PM_{2.5}$ indicated that HONO had a potential chemical link with haze particles.

Acknowledgments

This project was supported by the National Key Research and Development Program of China

365 (2016YFC0202700), and the National Natural Science Foundation of China (Contract No.
366 91544227); Z Shi is funded by NERC-MRC-NSFC Newton Fund (NE/N006992/1).

References

Acker, K., Febo, A., Trick, S., Perrino, C., Bruno, P., Wiesen, P., Moeller, D., Wieprecht, W., Auel, R., Giusto, M., Geyer, A., Platt, U., Allegrini, I., 2006. Nitrous acid in the urban area of Rome. Atmos. Environ. 40, 3123-3133.

Alicke, B., Platt, U., Stutz, J., 2002. Impact of nitrous acid photolysis on the total hydroxyl radical budget during the Limitation of Oxidant Production/Pianura Padana Produzione di Ozono study in Milan. J. Geophys. Res. Atmos. 107, 8196.

Ammann, M., Kalberer, M., Jost, D.T., Tobler, L., Rossler, E., Piguet, D., Gaggeler, H.W., Baltensperger, U., 1998. Heterogeneous production of nitrous acid on soot in polluted air masses. Nature 395, 157-160.

An, J.L., Li, Y., Chen, Y., Li, J., Qu, Y., Tang, Y.J., 2013. Enhancements of major aerosol components due to additional HONO sources in the North China Plain and implications for visibility and haze. Adv. Atmos. Sci. 30, 57-66.

Aumont, B., Chervier, F., Laval, S., 2003. Contribution of HONO sources to the $NO_x/HO_x/O_3$ chemistry in the polluted boundary layer. Atmos. Environ. 37, 487-498.

Bond, T.C., Doherty, S.J., Fahey, D.W., Forster, P.M., Berntsen, T., DeAngelo, B.J., Flanner, M.G., Ghan, S., Kärcher, B., Koch, D., Kinne, S., Kondo, Y., Quinn, P.K., Sarofim, M.C., Schultz, M.G., Schulz, M., Venkataraman, C., Zhang, H., Zhang, S., Bellouin, N., Guttikunda, S.K., Hopke, P.K., Jacobson, M.Z., Kaiser, J.W., Klimont, Z., Lohmann, U., Schwarz, J.P., Shindell, D., Storelvmo, T., Warren, S.G., Zender, C.S., 2013. Bounding the role of black carbon in the climate system: A scientific assessment. J. Geophys. Res. Atmos. 118, 5380-5552.

Broske, R., Kleffmann, J., Wiesen, P., 2003. Heterogeneous conversion of NO_2 on secondary organic aerosol surfaces: A possible source of nitrous acid (HONO) in the atmosphere? Atmos. Chem. Phys. 3, 469-474.

Che, H.Z., Xia, X.G., Zhu, J., Wang, H., Wang, Y.Q., Sun, J.Y., Zhang, X.Y., Shi, G.Y., 2015. Aerosol optical properties under the condition of heavy haze over an urban site of Beijing, China. Environ. Sci. Pollut. Res. Int. 22, 1043-1053.

Finlayson-Pitts, B.J., Wingen, L.M., Sumner, A.L., Syomin, D., Ramazan, K.A., 2003. The heterogeneous hydrolysis of NO_2 in laboratory systems and in outdoor and indoor atmospheres: An integrated mechanism. Phys. Chem. Chem. Phys. 5, 223-242.

George, C., Strekowski, R.S., Kleffmann, J., Stemmler, K., Ammann, M., 2005. Photoenhanced uptake of gaseous NO_2 on solid-organic compounds: a photochemical source of HONO? Faraday Discuss. 130, 195-210.

Guo, S., Hu, M., Zamora, M.L., Peng, J.F., Shang, D.J., Zheng, J., Du, Z.F., Wu, Z.J., Shao, M., Zeng, L.M., Molina, M.J., Zhang, R.Y., 2014. Elucidating severe urban haze formation in China. Proc. Natl. Acad. Sci. USA 111, 17373-17378.

He, H., Wang, Y.S., Ma, Q.X., Ma, J.Z., Chu, B.W., Ji, D.S., Tang, G.Q., Liu, C., Zhang, H.X., Hao, J.M., 2014. Mineral dust and NO_x promote the conversion of SO_2 to sulfate in heavy pollution days. Sci. Rep. 4, 4172.

Heard, D.E., Pilling, M.J., 2003. Measurement of OH and HO_2 in the troposphere. Chem. Rev. 103, 5163-5198.

Heland, J., Kleffmann, J., Kurtenbach, R., Wiesen, P., 2001. A new instrument to measure gaseous nitrous acid (HONO) in the atmosphere. Environ. Sci. Technol. 35, 3207-3212.

Hendrick, F., Muller, J.F., Clemer, K., Wang, P., De Maziere, M., Fayt, C., Gielen, C., Hermans, C., Ma, J.Z., Pinardi, G., Stavrakou, T., Vlemmix, T., Van Roozendael, M., 2014. Four years of ground-based MAX-DOAS observations of HONO and NO_2 in the Beijing area. Atmos. Chem. Phys. 14, 765-781.

Hofzumahaus, A., Rohrer, F., Lu, K.D., Bohn, B., Brauers, T., Chang, C.C., Fuchs, H., Holland, F., Kita, K., Kondo, Y., Li, X., Lou, S.R., Shao, M., Zeng, L.M., Wahner, A., Zhang, Y.H., 2009. Amplified trace gas removal in the troposphere. Science 324, 1702-1704.

Hou, S.Q., Tong, S.R., Ge, M.F., An, J.L., 2016. Comparison of atmospheric nitrous acid during severe haze and clean periods in Beijing, China. Atmos. Environ. 124, 199-206.

Hu, M., Zhou, F.M., Shao, K.S., Zhang, Y.H., Tang, X.Y., Slanina, J., 2002. Diurnal variations of aerosol chemical compositions and related gaseous pollutants in Beijing and Guangzhou. J. Environ. Sci. Health Part A Toxic/Hazard. Subst. Environ. Eng. 37, 479-488.

Huang, R.J., Yang, L., Cao, J., Wang, Q., Tie, X., Ho, K.F., Shen, Z., Zhang, R., Li, G., Zhu, C., Zhang, N., Dai, W., Zhou, J., Liu, S., Chen, Y., Chen, J., O'Dowd, C.D., 2017. Concentration and sources of atmospheric nitrous acid (HONO) at an urban site in Western China. Sci. Total Environ. 593-594, 165-172.

Huang, R.J., Zhang, Y., Bozzetti, C., Ho, K.F., Cao, J.J., Han, Y., Daellenbach, K.R., Slowik, J.G., Platt, S.M., Canonaco, F., Zotter, P., Wolf, R., Pieber, S.M., Bruns, E.A., Crippa, M., Ciarelli, G., Piazzalunga, A., Schwikowski, M., Abbaszade, G., Schnelle-Kreis, J., Zimmermann, R., An, Z., Szidat, S., Baltensperger, U., El Haddad, I., Prevot, A.S., 2014. High secondary aerosol contribution to particulate pollution during haze events in China. Nature 514, 218-222.

Jing, J.S., Wu, Y.F., Tao, J., Che, H.Z., Xia, X.G., Zhang, X.C., Yan, P., Zhao, D.M., Zhang, L.M., 2015. Observation and analysis of near-surface atmospheric aerosol optical properties in urban Beijing. Particuology 18, 144-154.

Kleffmann, J., 2007. Daytime sources of nitrous acid (HONO) in the atmospheric boundary layer. Chemphyschem 8, 1137-1144.

Kleffmann, J., Becker, K.H., Lackhoff, M., Wiesen, P., 1999. Heterogeneous conversion of NO_2 on carbonaceous surfaces. Phys. Chem. Chem. Phys. 1, 5443-5450.

Kleffmann, J., Gavriloaiei, T., Hofzumahaus, A., Holland, F., Koppmann, R., Rupp, L., Schlosser, E., Siese, M., Wahner, A., 2005. Daytime formation of nitrous acid: A major source of OH radicals in a forest. Geophys. Res. Lett. 32, L05818.

Kleffmann, J., Heland, J., Kurtenbach, R., Lorzer, J., Wiesen, P., 2002. A new instrument (LOPAP) for the detection of nitrous acid (HONO). Environ. Sci. Pollut. R. 4, 48-54.

Kurtenbach, R., Becker, K.H., Gomes, J.A.G., Kleffmann, J., Lorzer, J.C., Spittler, M., Wiesen, P., Ackermann, R., Geyer, A., Platt, U., 2001. Investigations of emissions and heterogeneous formation of HONO in a road traffic tunnel. Atmos. Environ. 35, 3385-3394.

Lammel, G., Cape, J.N., 1996. Nitrous acid and nitrite in the atmosphere. Chem. Soc. Rev. 25, 361-369.

Li, X., Brauers, T., Haeseler, R., Bohn, B., Fuchs, H., Hofzumahaus, A., Holland, F., Lou, S., Lu, K.D., Rohrer, F., Hu, M., Zeng, L.M., Zhang, Y.H., Garland, R.M., Su, H., Nowak, A., Wiedensohler, A., Takegawa, N., Shao, M., Wahner, A., 2012. Exploring the atmospheric chemistry of nitrous acid (HONO) at a rural site in Southern China. Atmos. Chem. Phys. 12, 1497-1513.

Li, Y., An, J.L., Min, M., Zhang, W., Wang, F., Xie, P.H., 2011. Impacts of HONO sources on the air quality in Beijing, Tianjin and Hebei Province of China. Atmos. Environ. 45, 4735-4744.

Liu, Y.C., Wu, Z.J., Wang, Y., Xiao, Y., Gu, F.T., Zheng, J., Tan, T.Y., Shang, D.J., Wu, Y.S., Zeng, L.M., Hu, M., Bateman, A.P., Martin, S.T., 2017a. Submicrometer particles are in the liquid state during heavy haze episodes in the urban atmosphere of Beijing, China. Environ. Sci. Technol. Lett. 4, 427-432.

Liu, Y.H., Lu, K.D., Ma, Y.F., Yang, X.P., Zhang, W.B., Wu, Y.S., Peng, J.F., Shuai, S.J., Hu, M., Zhang, Y.H., 2017b. Direct emission of nitrous acid (HONO) from gasoline cars in China determined by vehicle chassis dynamometer experiments. Atmos. Environ. 169, 89-96.

Lou, S., Holland, F., Rohrer, F., Lu, K., Bohn, B., Brauers, T., Chang, C.C., Fuchs, H., Häseler, R., Kita, K., Kondo, Y., Li, X., Shao, M., Zeng, L., Wahner, A., Zhang, Y., Wang, W., Hofzumahaus, A., 2010. Atmospheric OH reactivities in the Pearl River Delta – China in summer 2006: measurement and model results. Atmos. Chem. Phys. 10, 11243-11260.

Lu, K.D., Hofzumahaus, A., Holland, F., Bohn, B., Brauers, T., Fuchs, H., Hu, M., Haeseler, R., Kita, K., Kondo, Y., Li, X., Lou, S.R., Oebel, A., Shao, M., Zeng, L.M., Wahner, A., Zhu, T., Zhang, Y.H., Rohrer, F., 2013. Missing OH source in a suburban environment near Beijing: observed and modelled OH and HO_2 concentrations in summer 2006. Atmos. Chem. Phys. 13, 1057-1080.

Lu, K.D., Rohrer, F., Holland, F., Fuchs, H., Bohn, B., Brauers, T., Chang, C.C., Haeseler, R., Hu, M., Kita, K., Kondo, Y., Li, X., Lou, S.R., Nehr, S., Shao, M., Zeng, L.M., Wahner, A., Zhang, Y.H., Hofzumahaus, A., 2012. Observation and modelling of OH and HO_2 concentrations in the Pearl River Delta 2006: a missing OH source in a VOC rich atmosphere. Atmos. Chem. Phys. 12, 1541-1569.

Ma, J.Z., Chu, B.W., Liu, J., Liu, Y.C., Zhang, H.X., He, H., 2018. NO_x promotion of SO_2 conversion to sulfate: An important mechanism for the occurrence of heavy haze during winter in Beijing. Environ. Pollut. 233, 662-669.

Michoud, V., Kukui, A., Camredon, M., Colomb, A., Borbon, A., Miet, K., Aumont, B., Beekmann, M., Durand-Jolibois, R., Perrier, S., Zapf, P., Siour, G., Ait-Helal, W., Locoge, N., Sauvage, S., Afif, C., Gros, V., Furger, M., Ancellet, G., Doussin, J.F., 2012. Radical budget analysis in a suburban European site during the MEGAPOLI summer field campaign. Atmos. Chem. Phys. 12, 11951-11974.

Nakashima, Y., Sadanaga, Y., Saito, S., Hoshi, J., Ueno, H., 2017. Contributions of vehicular emissions and secondary formation to nitrous acid concentrations in ambient urban air in Tokyo in the winter. Sci. Total Environ. 592, 178-186.

Platt, U., Perner, D., 1980. Direct measurements of atmospheric CH_2O, HNO_2, O_3, NO_2, and SO_2 by differential optical-absorption in the near UV. J. Geophys. Res. 85, 7453-7458.

Qin, M., Xie, P.H., Liu, W.Q., Li, A., Dou, K., Fang, W., Liu, H.G., Zhang, W.J., 2006. Observation of atmospheric nitrous acid with DOAS in Beijing, China. J. Environ. Sci. China 18, 69-75.

Quan, J.N., Tie, X.X., Zhang, Q., Liu, Q., Li, X., Gao, Y., Zhao, D.L., 2014. Characteristics of heavy aerosol pollution during the 2012-2013 winter in Beijing, China. Atmos. Environ. 88, 83-89.

Rohrer, F., Berresheim, H., 2006. Strong correlation between levels of tropospheric hydroxyl radicals and solar ultraviolet radiation. Nature 442, 184-187.

Ropkins, K., DeFries, T.H., Pope, F., Green, D.C., Kemper, J., Kishan, S., Fuller, G.W., Li, H., Sidebottom, J., Crilley, L.R., Kramer, L., Bloss, W.J., Stewart Hager, J., 2017. Evaluation of EDAR vehicle emissions remote sensing technology. Sci. Total Environ. 609, 1464-1474.

Soergel, M., Regelin, E., Bozem, H., Diesch, J.M., Drewnick, F., Fischer, H., Harder, H., Held, A., Hosaynali-Beygi, Z., Martinez, M., Zetzsch, C., 2011. Quantification of the unknown HONO daytime source and its relation to NO_2. Atmos. Chem. Phys. 11, 10433-10447.

Spataro, F., Ianniello, A., 2014. Sources of atmospheric nitrous acid: state of the science, current research needs, and future prospects. J. Air Waste Manage. Assoc. 64, 1232-1250.

Spataro, F., Ianniello, A., Esposito, G., Allegrini, I., Zhu, T., Hu, M., 2013. Occurrence of atmospheric nitrous acid in the urban area of Beijing (China). Sci. Total Environ. 447, 210-224.

Stemmler, K., Ndour, M., Elshorbany, Y., Kleffmann, J., D'Anna, B., George, C., Bohn, B., Ammann, M., 2007. Light induced conversion of nitrogen dioxide into nitrous acid on submicron humic acid aerosol. Atmos. Chem. Phys. 7, 4237-4248.

Stutz, J., Alicke, B., Ackermann, R., Geyer, A., Wang, S.H., White, A.B., Williams, E.J., Spicer, C.W., Fast, J.D., 2004. Relative humidity dependence of HONO chemistry in urban areas. J. Geophys. Res. Atmos. 109, D03307.

Su, H., Cheng, Y.F., Cheng, P., Zhang, Y.H., Dong, S., Zeng, L.M., Wang, X., Slanina, J., Shao, M., Wiedensohler, A., 2008. Observation of nighttime nitrous acid (HONO) formation at a non-urban site during PRIDE-PRD2004 in China. Atmos. Environ. 42, 6219-6232.

Sun, Y.L., Jiang, Q., Wang, Z.F., Fu, P.Q., Li, J., Yang, T., Yin, Y., 2014. Investigation of the sources and evolution processes of severe haze pollution in Beijing in January 2013. J. Geophys. Res. 119, 4380-4398.

Tan, Z.F., Fuchs, H., Lu, K.D., Hofzumahaus, A., Bohn, B., Broch, S., Dong, H.B., Gomm, S., Haseler, R., He, L.Y., Holland, F., Li, X., Liu, Y., Lu, S.H., Rohrer, F., Shao, M., Wang, B.L., Wang, M., Wu, Y.S., Zeng, L.M., Zhang, Y.S., Wahner, A., Zhang, Y.H., 2017. Radical chemistry at a rural site (Wangdu) in the North China Plain: observation and model calculations of OH, HO_2 and RO_2 radicals. Atmos. Chem. Phys. 17, 663-690.

Tong, S.R., Hou, S.Q., Zhang, Y., Chu, B.W., Liu, Y.C., He, H., Zhao, P.S., Ge, M.F., 2016. Exploring the nitrous acid (HONO) formation mechanism in winter Beijing: direct emissions and heterogeneous production in urban and suburban areas. Faraday Discuss. 189, 213-230.

Tong, S.R., Hou, S.Q., Zhang, Y., Chu, B.W., Liu, Y.C., He, H., Zhao, P.S., Ge, M.F., 2015. Comparisons of measured nitrous acid (HONO) concentrations in a pollution period at urban and suburban Beijing, in autumn of 2014. Sci. China Chem. 58, 1393-1402.

Trinh, H.T., Imanishi, K., Morikawa, T., Hagino, H., Takenaka, N., 2017. Gaseous nitrous acid (HONO) and nitrogen oxides (NO_x) emission from gasoline and diesel vehicles under real-world driving test cycles. J. Air Waste Manag. Assoc. 67, 412-420.

Wang, J., Zhang, X., Guo, J., Wang, Z., Zhang, M., 2017. Observation of nitrous acid (HONO) in Beijing, China: Seasonal variation, nocturnal formation and daytime budget. Sci. Total Environ. 587-588, 350-359.

Wang, S., Zhou, R., Zhao, H., Wang, Z., Chen, L., Zhou, B., 2013. Long-term observation of atmospheric nitrous acid (HONO) and its implication to local NO_2 levels in Shanghai, China. Atmos. Environ. 77, 718-724.

Wong, K.W., Oh, H.J., Lefer, B.L., Rappenglueck, B., Stutz, J., 2011. Vertical profiles of nitrous acid in the nocturnal urban atmosphere of Houston, TX. Atmos. Chem. Phys. 11, 3595-3609.

Wu, Z.J., Hu, M., Shao, K., Slanina, J., 2009. Acidic gases, NH_3 and secondary inorganic ions in PM_{10} during summertime in Beijing, China and their relation to air mass history. Chemosphere 76, 1028-1035.

Yu, Y., Galle, B., Panday, A., Hodson, E., Prinn, R., Wang, S., 2009. Observations of high rates of NO_2-HONO conversion in the nocturnal atmospheric boundary layer in Kathmandu, Nepal. Atmos. Chem. Phys. 9, 6401-6415.

Yun, H., Wang, Z., Zha, Q.Z., Wang, W.H., Xue, L.K., Zhang, L., Li, Q.Y., Cui, L., Lee, S.C., Poon, S.C.N., Wang, T., 2017. Nitrous acid in a street canyon environment: sources and contributions to local oxidation capacity. Atmos. Environ. 167, 223-234.

Zhang, X.L., Mao, M., Berg, M.J., Sun, W.B., 2014. Insight into wintertime aerosol characteristics over Beijing. J. Atmos. Sol. Terr. Phys. 121, 63-71.